IET Microwaves, Antennas & Propagation

Research Article

IET Journals
The Institution of Engineering and Technology

Design of a broad-band microstrip loop antennas with less-dispersive group velocity for accurate direction finding

ISSN 1751-8725
Received on 16th July 2019
Revised 25th July 2019
Accepted on 29th July 2019
doi: 10.1049/iet-map.2019.0640
www.ietdl.org

Sungjun Yoo[1], Gangil Byun[2] ✉, Hosung Choo[1]

[1]*School of Electronic and Electrical Engineering, Hongik University, Seoul, Republic of Korea*
[2]*School of Electrical & Computer Engineering, Ulsan National Institute of Science and Technology (UNIST), Ulsan, Republic of Korea*
✉ *E-mail: byun@unist.ac.kr*

Abstract: This study proposes the design of broad-band microstrip loop antennas with less-dispersive group velocity of radiation patterns for accurate direction of arrival (DoA) estimation. The proposed structure consists of radiating and feeding microstrip loops, and the radiating loop is electromagnetically coupled to the feeding loop. This feeding mechanism helps to suppress phase variations of radiating patterns by avoiding dual resonances within a wide frequency band over 60 MHz, which allows to obtain the less-dispersive group velocity for accurate DoA estimation. The effectiveness of the less-dispersive behaviour is validated by implementing the proposed structure into a four-element array to estimate vertical and horizontal placements using dual-axis phase interferometry. The results confirm that the proposed antenna has less-dispersive group velocity compared to a conventional microstrip patch antenna and is more suitable for accurate DoA estimation.

1 Introduction

In high-speed aeronautic vehicles, phase interferometry has been widely used for direction finding (DF) systems due to its fast processing time and less computational loads [1–3]. Since these vehicles also require minimised air drag, a low-profile antenna array has been a suitable candidate as a front-end component, which measures phase differences in baselines using phase information of each element of array to estimate the direction of arrival of signal [4, 5]. These measured data are used to calculate correlations with pre-saved vectors of phase differences, and the direction of arrival (DoA) is estimated by the maximum correlation coefficient [6–8]. However, the phase difference becomes non-linear when each antenna of baselines experiences dispersion caused by surrounding environments, especially for broad-band sources. Thus, there have been a lot of efforts to acquire a higher precision of DoA through array configuration optimisation [9–13], DF algorithms [14–16], diversity characteristics of antennas [17, 18], and calibration methods [19–21]. In addition, antenna performances, such as bandwidth and mutual coupling characteristics, are enhanced for more accurate DoA estimation [22–25]. However, these efforts only provide practical solutions to compensate for the distorted phase variations and to improve antenna performances. In addition, there has not been an in-depth study on how to achieve less-dispersive phase variations from antenna engineering standpoints.

In this paper, the design of broad-band microstrip loop antennas is proposed to make an antenna with less-dispersive group velocity of radiation patterns for accurate DoA estimation. The less-dispersive group velocity is achieved to improve the DoA estimation performance using the in the interferometry DF system. The proposed structure consists of radiating and feeding microstrip loops that are printed on high-dielectric ceramic substrates. The feeding loop is connected to two output ports of a hybrid chip coupler for a quadratic phase excitation, and the radiating loop is electromagnetically fed by the feeding loop. Herein, the design parameters of the loops, such as diameters and strip widths, should be carefully tuned to prevent dual resonances within a target frequency band. Note that a drastic variation in group velocity occurs when two resonances are closely placed [26–28]. To validate the effectiveness of the less-dispersive behaviour, the proposed structure is adopted as individual elements of a four-element array. Then, DoAs are estimated by a dual-axis phase interferometry in vertical and horizontal directions. The reason for adopting the simple dual-axis phase interferometry is due to the system specifications. The dual-axis phase interferometry is designed to be mounted on low-cost missiles, requiring fast processing time and low computational complexity. In addition, four individual elements with dual-axis are the minimum number for estimating DoA in vertical and horizontal directions, while at the same time the simple interferometry with dual-axis is the DoA method requires the lowest computational complexity with the fast processing time. The proposed structure is further evaluated in comparison with a conventional microstrip patch antenna from various aspects: phase, phase difference, and group velocity. Also, the root-mean-square (RMS) error of the phase interferometry is observed for independent broad-band sources located between −45° and 45° in both azimuth and elevation. The results demonstrate that the proposed antenna with less-dispersive group velocity can be used for more accurate DoA estimation in DF system. The proposed interferometry DF antenna is suitable for simple low-cost DF applications such as small-sized missiles because the proposed antenna has been optimised to improve the estimation accuracy of DoA, especially when it is applied to a phase interferometry. Therefore, our antenna is designed to have a less-dispersive group velocity that is an important consideration in the simple interferometry method. Thus, the optimal performance cannot be guaranteed when the proposed antenna is applied to systems using other algorithms, such as MUSIC, ESPRIT, and Pseudo Doppler.

2 Proposed antenna structure

Figs. 1*a* and *b* show the geometry of the proposed antenna that consists of a radiating loop, a feeding loop, and a printed circuit board (PCB). Each microstrip loop is printed on a high-dielectric ceramic substrate ($\varepsilon_r = 20$, $\tan\delta = 0.0035$) with thickness h_1 and diameter g_r. The circumference and the strip width of the radiating loop are adjusted by parameters r_1 and r_2, and those of the feeding loop are varied by r_3 and r_4. The feeding loop is directly connected to two output ports of a hybrid chip coupler at the feeder, and the position of the feeder is specified f_x and f_y. The radiating loop is fed by the feeding loop through near electromagnetic fields, and the design parameters are tuned to achieve a less-dispersive behaviour within the frequency range from 1545 to 1605 MHz, which is often occupied by intentional chirp jammers. Note that the key design scheme is to resonate only the radiating loop while avoiding an

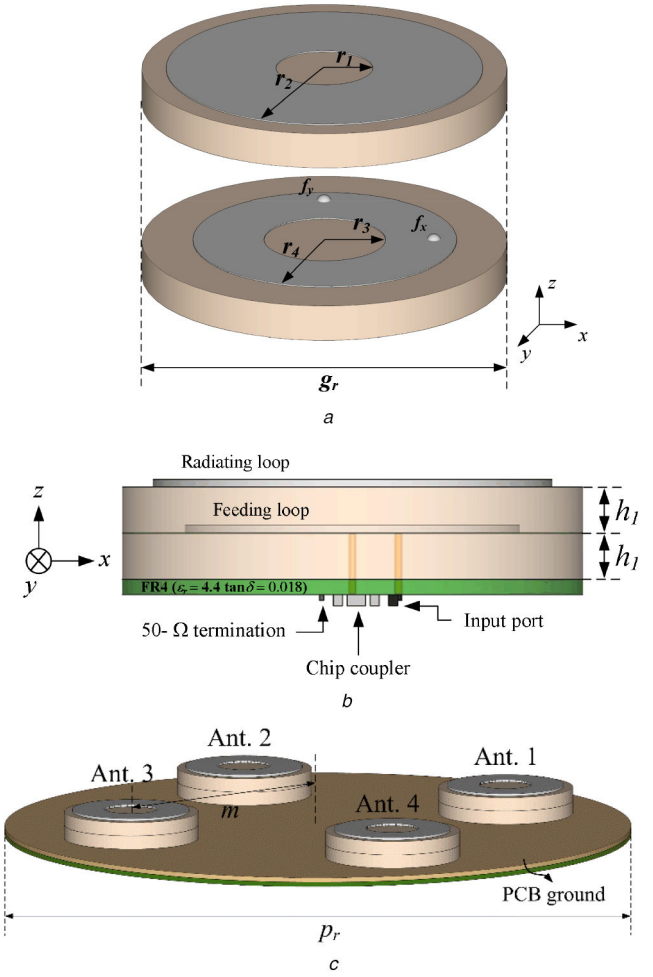

Fig. 1 *Geometry of the four-element array with the proposed broad-band microstrip loop antennas*

(a) Design parameters of microstrip loops, ***(b)*** Side projection view of a stand-alone antenna, ***(c)*** Perspective view of the four-element array

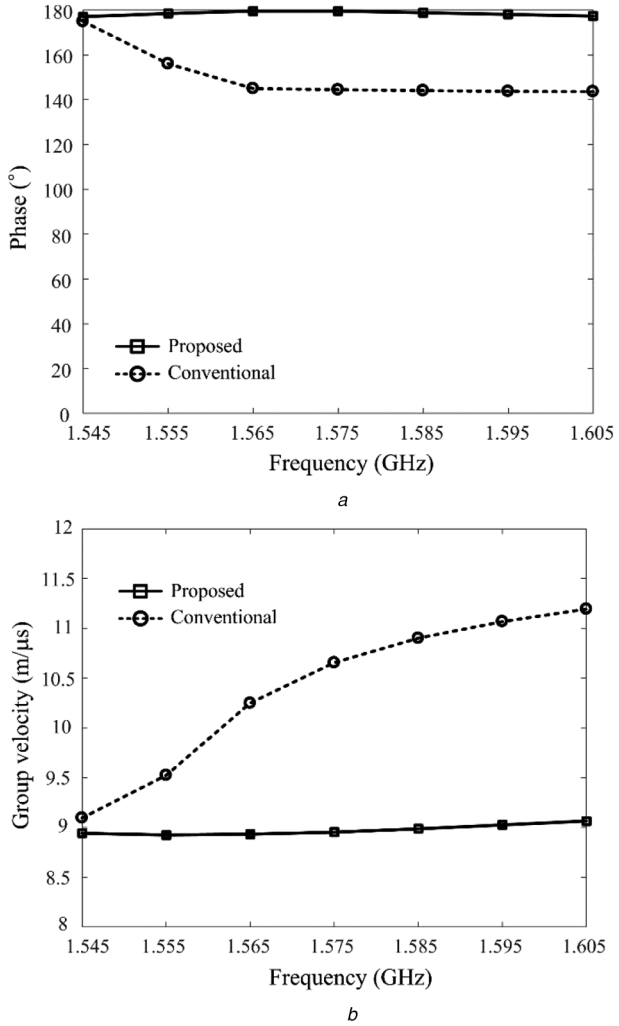

Fig. 2 *Comparison of the phase and group velocity properties between the proposed and conventional antenna*

(a) Phase property, ***(b)*** Group velocity property

additional resonance of the feeding loop within the target frequency band. This scheme prevents drastic phase variations with respect to frequency, which results in the less-dispersive group velocity, and also allows to a broadband circular polarisation (CP) bandwidth as well as broadband matching bandwidth.

Fig. 1*c* shows the geometry of a four-element array, and its identical elements are arranged at a distance m from the centre. To excite each antenna with quadrature phases, some circuits such as hybrid chip couplers, 50-Ω termination chips, and microstrip transmission lines are integrated into the PCB ground with diameter p_r. In our dual-axis phase interferometry, Ant. 1 and Ant. 3 are used to estimate elevation angles, while Ant. 2 and Ant. 4 find azimuth directions of incoming signals.

Fig. 2 presents the phase variations and the group velocity in the target frequency band. The properties of the proposed structure are compared with a conventional microstrip patch antenna that has two truncated corners for CP. The edge length of the patch is 18 mm, and the two corners are truncated by 4.8 mm. The shape of the patch is printed on a ceramic substrate (30 mm × 30 mm × 8 mm, $\varepsilon_r = 20$, $\tan\delta = 0.0035$), and the patch is fed by a coaxial probe at 3.7 mm off the centre. As can be seen, the phase variation of the proposed antenna is less than 5° in the target frequency band, on the other hand, the conventional antenna has a larger variation of 30°. This leads to different behaviours of the group velocity that is defined by

$$v_g = \frac{\partial w}{\partial k} \tag{1}$$

where w is the wave's angular frequency, and k is the wave number. Since the group velocity is calculated based on the phase information, the proposed antenna has an almost steady value of about 8.9 m/μs over the target frequency band.

Note that the value of the conventional antenna increases from 9.1 to 11 m/μs, and the effect of this variance will be observed in Section 3.2.

3 Verification of the proposed antenna

3.1 Measured antenna characteristics

Fig. 3*a* presents a photograph of a fabricated four-element array with the PCB ground, and detailed values of the design parameters are listed in Table 1. As aimed, the effective feeding and radiating loops have loop lengths of 46.9 and 42.4 mm, which is about one effective wavelength at 1.43 and 1.58 GHz, respectively. The proposed antenna is particularly optimised to have less-dispersive group velocity for the phase interferometry. When the proposed antenna structure is applied to other algorithms, the detailed design parameters of the antenna can be slightly changed depending on the applied DoA algorithms. Fig. 3*b* shows the bottom of the PCB that includes four hybrid chip couplers, 50-Ω terminations, coplanar wave guides, and coaxial cables.

Fig. 4 shows a comparison of the measured and simulated reflection coefficients. The measured data are obtained when Ant. 1 is fed by a coaxial cable, while other elements are terminated by 50-Ω loads. The simulated values are calculated using Advanced Design Software (ADS) to consider the four-port network of the hybrid chip coupler in conjunction with a 2 × 2 scattering matrix of the antenna, which is computed by the FEKO EM simulator [29, 30]. The measured reflection coefficients are specified by a solid line and have an average value of −14.2 dB over the 60-MHz

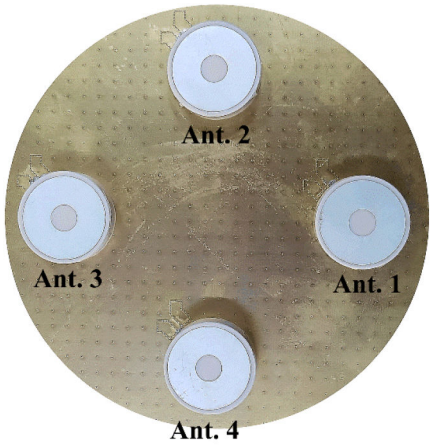

a

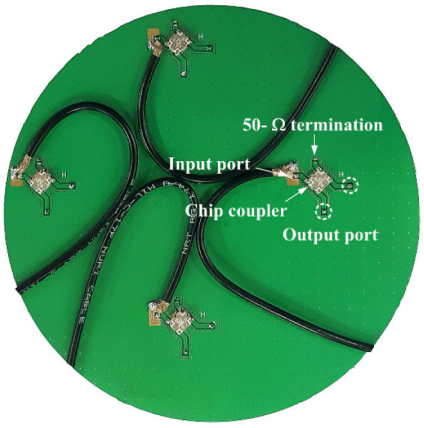

b

Fig. 3 *Photographs of the fabricated four-element array and the PCB ground*
(a) Top view, ***(b)*** Bottom view

Table 1 Design parameter of the fabricated antenna

Parameter	Value
r_1	4.2 mm
r_2	13 mm
r_3	5.1 mm
r_4	12.3 mm
f_x	(8.7 mm, 0 mm)
f_y	(0 mm, 8.7 mm)
g_r	29 mm
h_1	6 mm
h_2	6 mm
m	46.7 mm

bandwidth from 1.545 to 1.605 GHz. The dashed line indicates the simulated result and shows a similar tendency with the measured data with an average value of −15.4 dB.

Fig. 5 presents measured mutual coupling in comparison with the simulated data. Mutual coupling is maintained to be lower than −12.7 dB between 1.545 and 1.605 GHz, and S_{12}, S_{13}, and S_{14} averaged over the frequency range are −16.6, −26.2, and −25.7 dB for measurement and −21.3, −20.7, and −18.6 dB for simulation, respectively.

Fig. 6 shows a comparison between the measured and simulated bore-sight gains of the Ant. 1. The values are calculated using active element patterns at $\theta = 0°$, and the solid line indicates the simulated results. The measured data are obtained from a full anechoic chamber and are specified by ' + ' markers. The measured value at 1.575 GHz is 0.58 dBic, and the gain is greater than −1

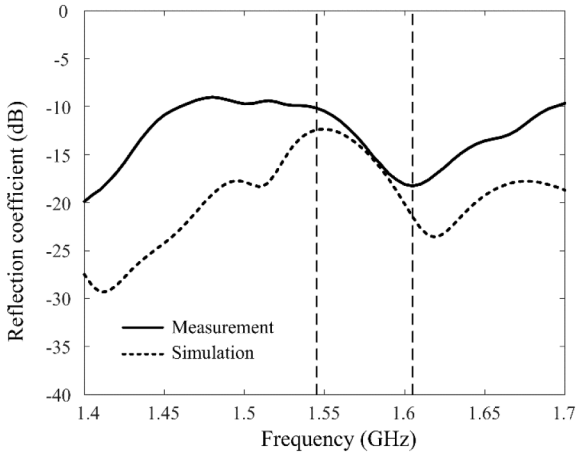

Fig. 4 *Measured and simulated reflection coefficients as a function of frequency*

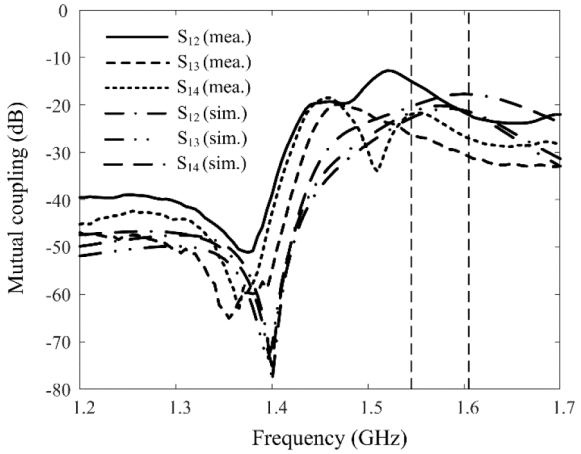

Fig. 5 *Comparison of measured and simulated mutual coupling between antennas of the four-element array*

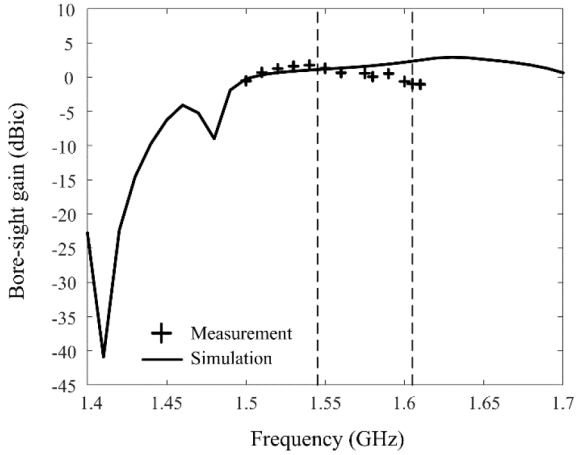

Fig. 6 *Measured and simulated bore-sight gains of the proposed antenna*

dBic in the 60-MHz bandwidth, and the gain deviation between 1.5 and 1.7 GHz (200 MHz) is <0.91 dB.

Fig. 7 exhibits a comparison of measured and simulated axial ratios (ARs) of Ant. 1, and these values are also computed from active element patterns in the bore-sight direction. Measured and simulated ARs are 2.1 and 2.2 dB at 1.575 GHz, and their average values are 1.98 and 2.4 dB in the frequency range. The antenna is circularly polarised with ARs of <3 dB, which implies that the phase information of the radiating patterns is not significantly distorted in the presence of mutual coupling.

Figs. 8*a* and *b* present the measured and simulated radiation patterns in *zx*- and *zy*- planes at 1.575 GHz. In the *zx*-plane, the measured half power beam width (HPBW) is 111°, and the

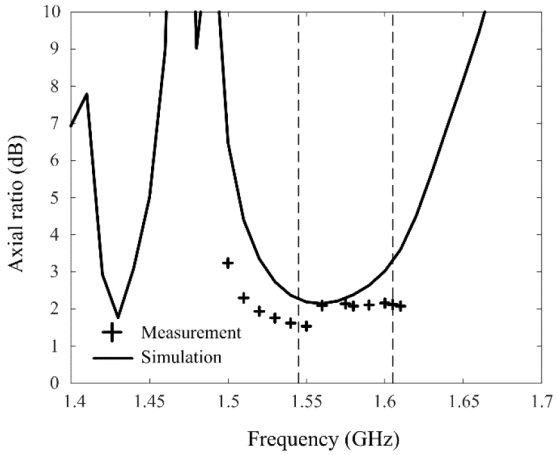

Fig. 7 *Measured and simulated ARs as a function of frequency*

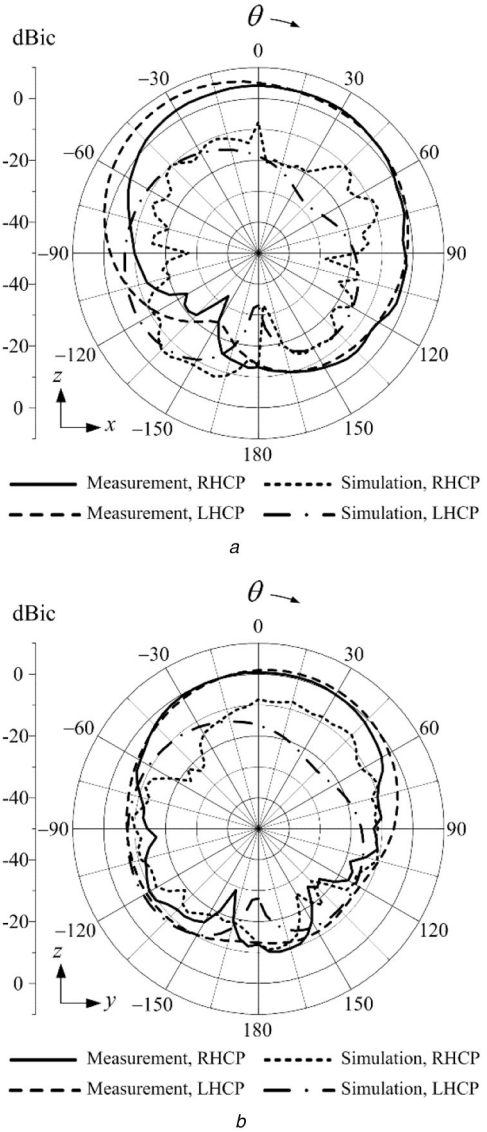

Fig. 8 *Measured and simulated 2D radiation patterns at 1.575*
(a) Patterns in the *zx*-plane, ***(b)*** Patterns in the *zy*-plane

maximum gain is observed at $\theta = 0°$ with a value of 0.58 dBic. The HPBW in the *zy*-plane is 94°, and the maximum value of 0.65 dBic is located at $\theta = -5°$. Figs. 9*a* and *b* show the radiation patterns at 1.605 GHz. Measured HPBWs are 113° and 99.5° in the *zx*- and *zy*-planes, and simulated HPBWs are 91.9° and 91.1° in the *zx*- and *zy*-planes, respectively. As expected, the proposed antenna does not exhibit any serious pattern distortion in the upper hemisphere with HPBWs of >90°.

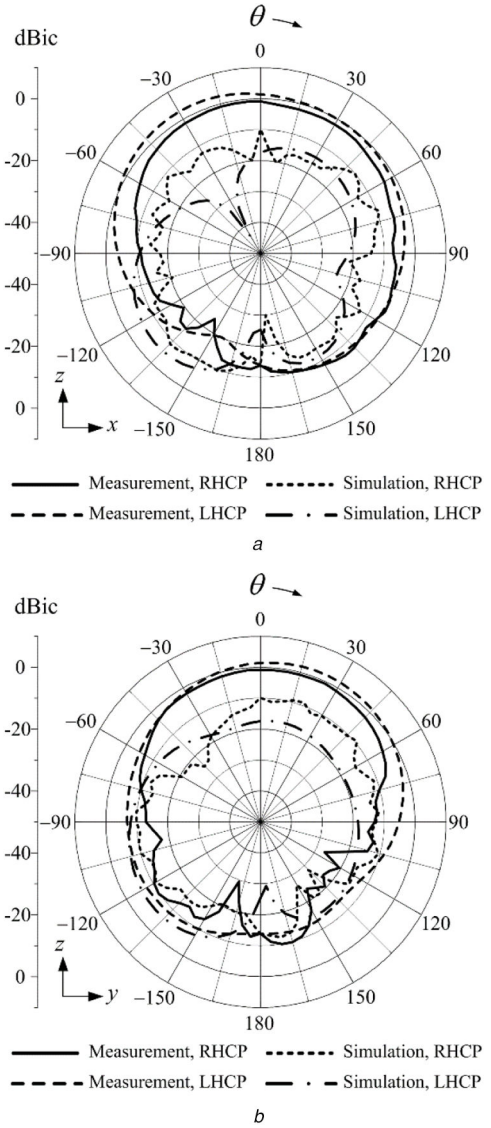

Fig. 9 *Measured and simulated 2D radiation patterns at 1.605*
(a) Patterns in the *zx*-plane, ***(b)*** Patterns in the *zy*-plane

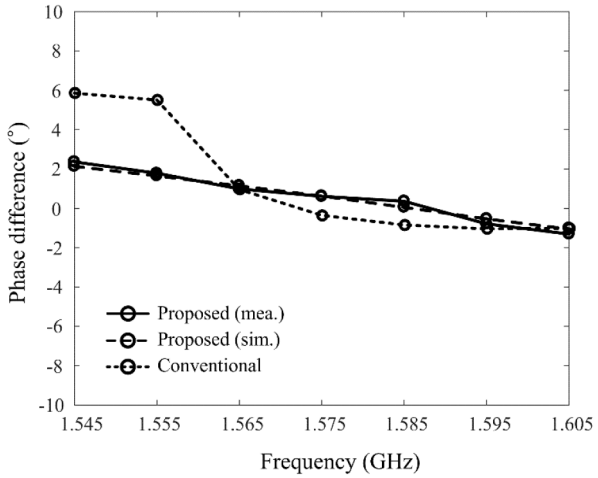

Fig. 10 *Measured and simulated phase differences of the proposed antenna in comparison with the conventional antenna*

3.2 Dual-axis phase interferometry

To validate the effectiveness of the proposed antenna, phase differences between Ant. 1 and Ant. 3 are calculated using active element patterns at $\theta = 0°$ and are compared with the conventional antenna, as shown in Fig. 10. For a fair comparison, the

conventional antenna is tuned for the same ceramic substrate ($\varepsilon_r = 20$, $\tan\delta = 0.0035$), and four identical elements are arranged at the same distance m from the centre. As anticipated, phase differences of the conventional antenna significantly increase in the lower frequency band with the maximum deviation of 5.8°. On the other hand, the phase differences of the proposed antenna are almost linear, and the maximum deviation decreases to 2.3° for measurement and 2.1° for simulation.

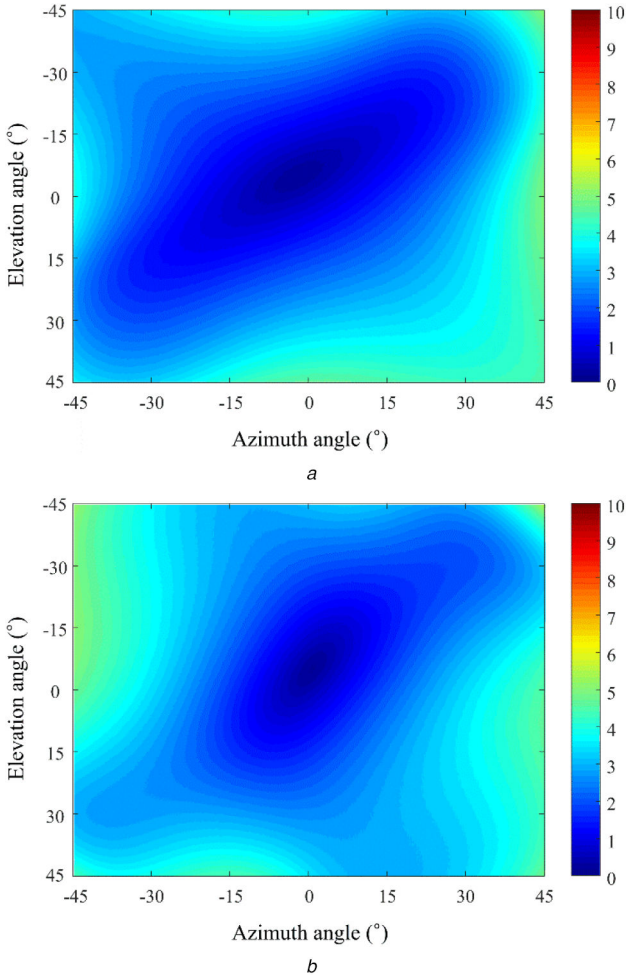

Fig. 11 *Comparison of the RMS error obtained using the phase interferometer at 1.575 GHz*
(a) RMS error of the proposed array, ***(b)*** RMS error of the conventional array

Table 2 DoA estimation error according to the frequency

Frequency, GHz	Proposed average (max)	Conventional average (max)
1.545	2.1° (8.1°)	4.9° (9.3°)
1.555	2.0° (8.0°)	4.1° (9.8°)
1.565	1.8° (7.2°)	3.7° (8.7°)
1.575	1.7° (6.6°)	4.0° (8.3°)
1.585	1.7° (6.3°)	4.7° (11.3°)
1.595	1.6° (6.1°)	5.8° (14.3°)
1.605	1.7° (5.8°)	7.2° (16.9°)

Fig. 11 shows a comparison of the RMS error calculated by varying DoAs that are estimated using a correlation vector direction finding (CVDF) algorithm [31]. In phase interferometry using CVDF, an array manifold, containing phase difference information between elements is precomputed according to the incident angles to achieve a pre-saved set of steering vectors, and the DoA of signal can be estimated by comparing the phase difference of the received signal with the pre-saved steering vectors.

It is assumed that independent incoming signals are located from −45° to 45° at intervals of 0.1° in both azimuth and elevation, and the signal-to-noise ratio is −30 dB. For each incoming signal, we iterate 100 times to calculate an average value to obtain more reliable results. As can be seen, accurate DoA estimation is possible near the bore-sight direction ($\phi = 0°$, $\theta = 0°$) with the RMS error close to zero for both arrays; however, the error tends to increase as the incident angle becomes larger. For example, the error values of the proposed and conventional antennas at $\phi = -45°$ and $\theta = -45°$ are increased to 2.9° and 5.2°. The proposed antenna shows an average RMS error of 1.8° with the maximum value of 6.1°. These values are even higher in the conventional antenna array with an average value of 4.0° and the maximum value of 8.2°. Table 2 presents variations of the RMS error according to the frequency. The results show that the less-dispersive behaviour of the group velocity prevents a significant phase distortion in the 60-MHz bandwidth, which results in lower RMS error for the DoA estimation. Table 3 shows the target frequency, polarisation, number of elements of array, antenna size, and RMS error in comparison with other existing researches presented in [11, 13, 17, 23]. The proposed antenna size is small compared to the previous researches while the RMS error maintains about 1.7°, which supports the effectiveness of the proposed approach. In the future research, we will adopt a larger number of elements, such as 6 or 8-element array and the effect of different element spacing will be considered to improve the accuracy of DoA estimation. In addition, the DoA performance will be analysed when the proposed antenna structure is applied for other algorithms, such as MUSIC, ESPRIT, and Pseudo Doppler.

4 Conclusion

Design of broad-band microstrip loop antennas has investigated to obtain less-dispersive group velocity of radiation patterns. The feeding loop is connected to hybrid chip coupler for the quadratic excitation, and the radiating loop is fed by the feeding loop through near electromagnetic fields. In our design, diameters and widths of the loops were carefully determined to obtain the less-dispersive group velocity by avoiding the dual resonance within the target frequency band. This less-dispersive behaviour of the proposed antenna structure was verified by measuring antenna characteristics. The measured bore-sight gain was 0.58 dBic at 1.575 GHz, and the gain deviation was <0.91 dB (from 1.5 to 1.7 GHz) in the four-element array. The proposed antenna showed the maximum phase difference of 2.3° in the target band, which was much lower than the conventional antenna. Then, the proposed antenna for the four-element array was employed to estimate DoAs using the dual-axis phase interferometry. The results demonstrate that the proposed antenna is suitable for more accurate DoA estimation with an improved average RMS error of 2.2°, and maximum value of 2.1°.

Table 3 Comparison of array antenna performance to existing results in the literature

No.	Target frequency, GHz	Pol.	No. of elements	Size (λ_0) in centre frequency	RMS error (average)
[11]	—	LP	4	—	6.0°
[13]	1.227, 1.575	CP	1 (differential pattern)	0.34 × 0.34 × 0.25	1.8°
[17]	2.2–3.4	LP	4	1.42 × 1.42 × 0.7	2.0°
[23]	1.6–3.2	LP	6	—	1.0°
prop.	1.545–1.605	CP	4	0.15 × 0.15 × 0.03	1.7°

5 Acknowledgments

This work was supported by the National Research Foundation of Korea (NRF) grant funded by the Korea government (MSIP) (no. NRF-2017R1A5A1015596) and the Basic Science Research Program through the National Research Foundation of Korea (NRF) funded by the Ministry of Education (no. 2015R1A6A1A03031833).

6 References

[1] Yu, N., Qi, X.H., Qiao, X.L.: 'Multi-channels wideband digital reconnaissance receiver based on compressed sensing', *IET Signal Process.*, 2013, **7**, (8), pp. 731–742

[2] Lui, H.-S., Hui, H.T.: 'Direction-of-arrival estimation: measurement using compact antenna arrays under the influence of mutual coupling', *IEEE Antennas Propag. Mag.*, 2015, **57**, (6), pp. 62–68

[3] Wu, Y.-W., Rhodes, S., Satorius, E.H.: 'Direction of arrival estimation via extended phase interferometry', *IEEE Trans. Aerosp. Electron. Syst.*, 1955, **31**, (1), pp. 375–381

[4] Hirata, A., Morimoto, T., Kawasaki, Z.: 'DOA estimation of ultra-wideband EM waves with MUSIC and interferometry', *IEEE Antennas Wireless Propag. Lett.*, 2003, **2**, (1), pp. 190–193

[5] Morimoto, T., Hirata, A., Kawasaki, Z.: 'Direction-of-arrival estimation for ultra-wideband EM waves with an interferometry', *Microw. Opt. Tech. Lett.*, 2003, **37**, (1), pp. 17–18

[6] Blunt, S.D., Chan, T., Gerlach, K.: 'Robust DOA estimation: the reiterative superresolution (RISR) algorithm', *IEEE Trans. Aerosp. Electron. Syst.*, 2011, **47**, (1), pp. 332–346

[7] Karasalo, I.: 'Estimating the covariance matrix by signal subspace averaging', *IEEE Trans. Aerosp. Signal Process.*, 1986, **ASSP-34**, (1), pp. 8–12

[8] Schmidt, R.O.: 'Multiple emitter location and signal parameter estimation', *IEEE Trans. Antennas Propag.*, 1986, **P-34**, (1), pp. 276–280

[9] Musselman, R.L., Norgrad, J.D.: 'Frequency invariant interferometry', *IEEE Trans. Electromagn. Compat.*, 1992, **34**, (2), pp. 86–92

[10] Gavish, M., Weiss, J.: 'Array geometry for ambiguity resolution in direction finding', *IEEE Trans. Antennas Propag.*, 1996, **44**, (6), pp. 889–895

[11] Liao, B., Chan, S.-C.: 'Direction-of-arrival estimation in subarrays-based linear sparse arrays with gain/phase uncertainties', *IEEE Trans. Aerosp. Signal Process.*, 2013, **49**, (4), pp. 2268–2280

[12] Byun, G., Hyun, J.-C., Seo, S.M., *et al.*: 'Optimum array configuration to improve null steering time for mobile CRPA systems', *J. Electromagn. Eng. Sci.*, 2016, **16**, (2), pp. 74–79

[13] Kataria, C., Gao, G., Bernhard, J.: 'Design of a compact hemispiral GPS antenna with direction finding capabilities', *IEEE Trans. Antennas Propag.*, 2019, **67**, (5), pp. 2878–2885

[14] Ward, D.B., Ding, Z., Kennedy, A.: 'Broadband DOA estimation using frequency invariant beamforming', *IEEE Trans. Signal Process.*, 1998, **46**, (5), pp. 1463–1469

[15] Santiago, E.A., Saquib, M.: 'Noise subspace-based iterative technique for direction finding', *IEEE Trans. Aerosp. Electron. Syst.*, 2013, **49**, (4), pp. 2281–2295

[16] Tian, Y., Xu, H.: 'Extended-aperture DOA estimation with unknown number of sources', *Electron. Lett.*, 2015, **51**, (7), pp. 583–584

[17] Duplouy, J., Morlaas, C., Aubert, H., *et al.*: 'Wideband and reconfigurable vector antenna using radiation pattern diversity for 3-D direction-of-arrival estimation', *IEEE Trans. Antennas Propag.*, 2019, **67**, (6), pp. 3586–3596

[18] Ferrara, E., Parks, T.: 'Direction finding with an array of antennas having diverse polarizations', *IEEE Trans. Antennas Propag.*, 1983, **31**, (2), pp. 231–236

[19] Dandekar, K.R., Ling, H., Xu, G.: 'Mutual coupling calibration for microstrip antenna arrays via element pattern reconstruction method', *IEEE Trans. Wirless Commun.*, 2014, **13**, (1), pp. 51–54

[20] Dandekar, K.R., Ling, H., Xu, G.: 'DOA estimation of coherent signals based on direct data domain under unknown mutual coupling', *IEEE Antennas Wireless Propag. Lett.*, 2014, **13**, (1), pp. 1525–1528

[21] Malik, W.Q., Stevens, C.J., Edwards, D.J.: 'Ultrawideband antenna distortion compensation', *IEEE Trans. Antennas Propag.*, 2008, **56**, (7), pp. 1900–1907

[22] Dandekar, K.R., Ling, H., Xu, G.: 'Experimental study of mutual coupling compensation in smart antenna applications', *IEEE Trans. Wirless Commun.*, 2002, **1**, (3), pp. 480–487

[23] Wang, B.H., Hui, H.T.: 'Wideband mutual coupling compensation for receiving antenna arrays using the system identification method', *IET Microw. Antennas Propag.*, 2011, **5**, (2), pp. 184–191

[24] Lin, M., Yang, L.: 'Blind calibration and DOA estimation with uniform circular arrays in the presence of mutual coupling', *IEEE Antennas Wireless Propag. Lett.*, 2006, **5**, pp. 315–318

[25] Rubio, J., Izquierdo, J.F., Córcoles, J.: 'Mutual coupling compensation matrices for transmitting and receiving arrays', *IEEE Trans. Antennas Propag.*, 2015, **63**, (2), pp. 839–843

[26] Hall, P.S., Dahele, J.S., James, J.R.: 'Design principles of sequentially fed, wide bandwidth, circularly polarized microstrip antennas', *IET Microw. Antennas Propag.*, 1989, **136**, (5), pp. 381–389

[27] Soon, C., Davis, L.E.: 'A comparison of the phase shift characteristics of axially-magnetized microstrip and slotline on ferrite', *IEEE Trans. Magn.*, 1995, **31**, (6), pp. 3464–3466

[28] Foroozesh, A., Shafai, L.: 'Investigation into the effects of the reflection phase characteristics of highly-reflective superstrates on resonant cavity antennas', *IEEE Trans. Antennas Propag.*, 2010, **58**, (10), pp. 3392–3396

[29] Advanced design system (ADS), Keysight, 2018, Available at http://www.keysight.com, accessed 5 September 2018

[30] FEKO, Altair, 2018. Available at http://www.altair.com, accessed 5 September 2018

[31] He, J., Liu, Z.: 'Two-dimensional direction finding of acoustic sources by a vector sensor array using the propagator method', *Signal Process.*, 2008, **88**, (10), pp. 2492–2499